JOURNAL OF AIRCRAFT
Vol. 46, No. 4, July–August 2009

Active Flow Control for Practical High-Lift Systems

Arvin Shmilovich* and Yoram Yadlin†
The Boeing Company, Huntington Beach, California 92647

DOI: 10.2514/1.41236

The application of active flow control for high-lift multi-element wing sections is investigated. A computational fluid dynamics procedure is used to simulate the interactive flow in conjunction with distributed flow control. Favorable nonlinear interactions using flow control on a conventional wing section and an advanced airfoil lead to major aerodynamic performance improvements at representative takeoff and landing conditions. This study demonstrates that judicious application of flow control at select locations on the individual wing elements may lead to near inviscid lift levels in the linear lift range and substantial gains in maximum lift.

Nomenclature

c	=	chord length
C_D	=	drag coefficient
C_L	=	lift coefficient
$C_{L\max}$	=	maximum lift coefficient
C_μ	=	slot momentum coefficient, $(h/c)\cdot(\rho_j/\rho_\infty)\cdot(U_j/U_\infty)^2$
f	=	actuator frequency, Hz
F^+	=	reduced forcing frequency, $f\cdot c/U_\infty$
h	=	actuator slot width
L/D	=	lift-to-drag ratio
M_j	=	peak jet Mach number
P_T	=	total pressure
P_{T_∞}	=	freestream total pressure
U_j	=	peak jet velocity
U_∞	=	freestream velocity
α	=	angle of attack
δ_{Flap}	=	flap deflection angle
ρ_j	=	jet density
ρ_∞	=	freestream density

I. Introduction

IN RECENT years a variety of flow control techniques have been developed for a wide range of applications [1–8]. Significant breakthroughs have been achieved using active flow control (AFC) for improved aerodynamic performance by reducing flow separation. A review of flow control applications for various body shapes and simple airfoils is given by Wygnanski [4]. Several studies were geared toward demonstrating the effectiveness of pulsed actuation in controlling the leading-edge flow separation, which occurs for airfoils at high angles of attack [9–14]. Other examples include airfoil sections with relatively simplified high-lift devices [15–18], that is, drooped leading edges and simple hinge flap elements (nonslotted flaps). Recently, a high-lift configuration has been investigated by using an actuation port on the slotted flap, demonstrating gains of 10–12% in lift [19].

Although significant inroads have been made in the context of relatively simple airfoil shapes, the question of whether AFC could be integrated into a practical airplane design is still outstanding. This is crucial for airframe manufacturers because one of the principal design objectives of commercial and military airplanes is to achieve mission requirements for takeoff and landing. Because superior high-

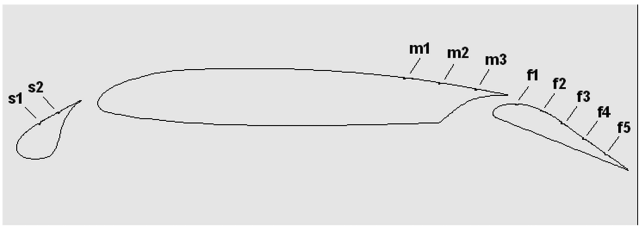

a) Conventional section takeoff position, δ_{Flap} = 24° AFC (2,3,5) port layout

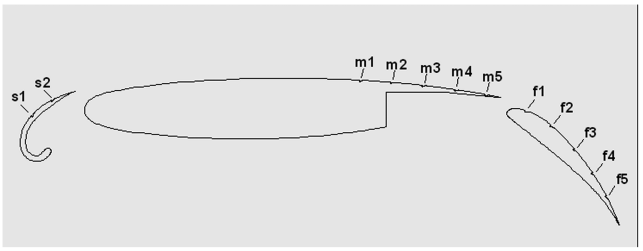

b) Advanced section landing position, δ_{Flap} = 50° AFC (2,5,5) port layout

Fig. 1 Port layout for the multi-element wing sections.

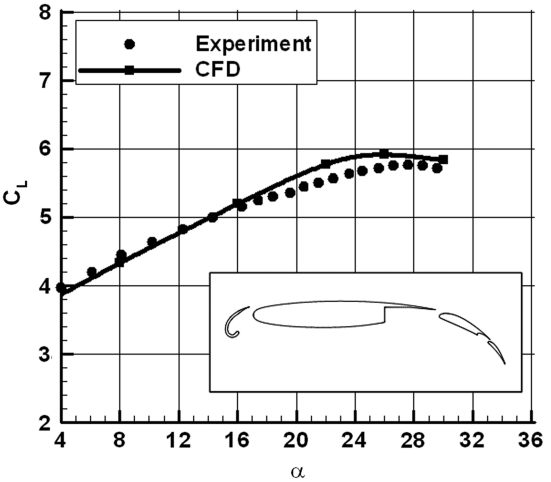

Fig. 2 Validation of the computational tool for a multi-element wing section without AFC (forerunner to the advanced section).

Presented as Paper 3971 at the 37th AIAA Fluid Dynamics Conference and Exhibit, Miami, FL; received 25 September 2008; revision received 13 November 2008; accepted for publication 16 November 2008.

*Technical Fellow, Aerodynamic Technology, 5301 Bolsa Avenue, Mail Stop H45N-E405. Senior Member AIAA.

†Senior Engineer/Scientist, Aerodynamic Technology, 5301 Bolsa Avenue, Mail Stop H45N-E405. Senior Member AIAA.

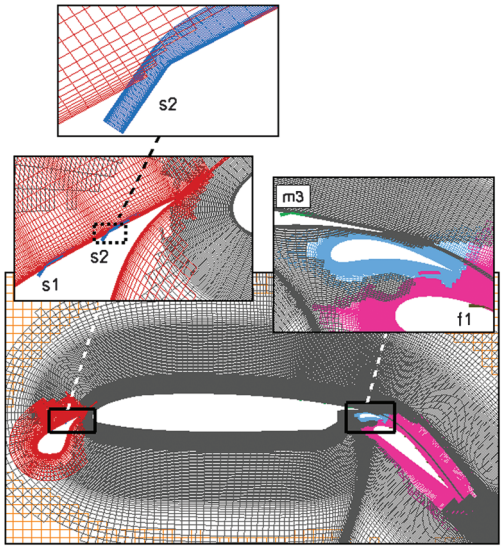

Fig. 3 Grid system for the conventional section in landing configuration ($\delta_{Flap} = 40$ deg).

lift capability is a key objective at these flight conditions, current airplanes employ multi-element systems in order to produce the necessary lift levels. It is therefore important to assess the merit of AFC for configurations, which have already been optimized for high lift and to establish performance increments due to flow control. The current study is aimed at identifying potential implementations of flow control for multi-element wing sections and providing guidelines on practical modes of actuation. Computational fluid dynamics (CFD) simulations are used to assess AFC performance improvements. CFD modeling is especially important in scenarios involving multi-element high-lift systems and flow control devices where alternative wind-tunnel testing is extremely expensive and often impractical.

This paper will first address the challenges associated with AFC implementation for multi-element high-lift configurations. The current analysis strategy will be described and techniques of flow diagnostics in the context of time-varying flow control actuation will be presented. A systematic process is employed for evaluating the application of flow control for two different, but representative, multi-element wing sections. The utility of AFC over the practical range of angles of attack will be established, and methods of exploiting certain actuation patterns for given performance levels will be explored.

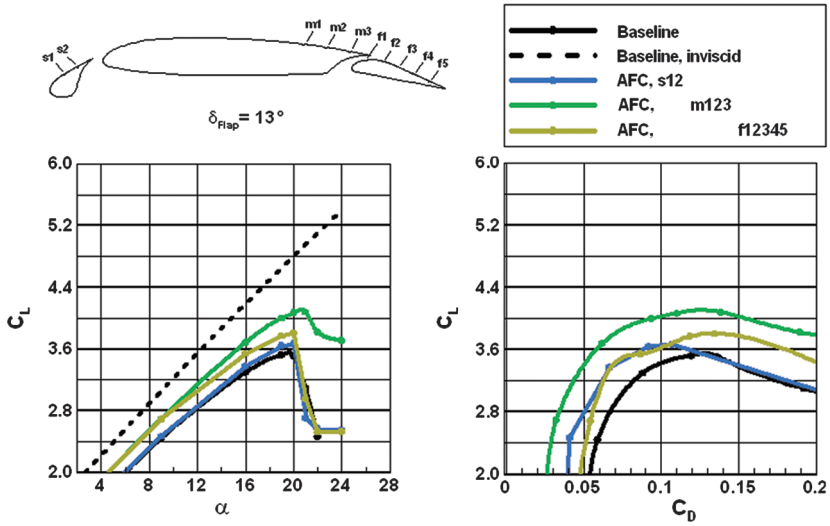

a) Actuation at individual wing components

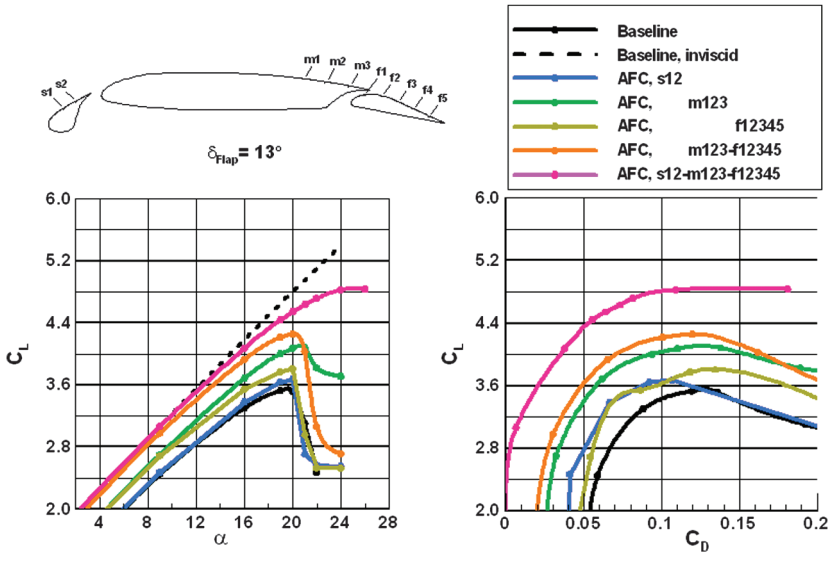

b) Combined actuation

Fig. 4 AFC for the conventional wing section at takeoff flap of 13 deg.

II. Active Flow Control Implementation

Various AFC implementations are investigated by considering general flow characteristics about multi-element configurations.

A. Multi-Element Wing Systems

Takeoff and landing distances are strongly dependent on airplane stall speed. Low stall speed is highly desirable because it allows the use of shorter field lengths. For given airplane weight it is possible to reduce stall speed by either increasing wing area or increasing the maximum lift coefficient. Increasing the wing area is undesirable because it results in higher cruise drag. It is more desirable to increase $C_{L\max}$ instead. Current airplanes achieve high levels of lift by employing systems that are deployed only during takeoff and landing. These systems usually consist of a movable leading-edge slat and trailing-edge flaps. When deployed, the wing transforms into a multi-element configuration, effectively increasing camber and chord length and resulting in added lift.

The flow over a multi-element high-lift system is highly interactive. For instance, the trailing-edge flap is strongly influenced by the downwash generated by the lift on the main wing. Conversely, the lift on the flap induces upwash on the slat and main wing. Several factors can limit the maximum lift that can be achieved by a multi-element system. The maximum lift is limited by viscous effects resulting from the very strong pressure gradients introduced by the high suction levels. Or, it can be limited by boundary-layer separation in the vicinity of the slat and main wing leading edge. It can also be limited by boundary-layer thickening or separation on the trailing edge of the main wing or on the flap elements. Another limitation can occur due to bursting of the viscous wake from the slat or the main wing as it passes through the high-pressure gradients developed by the flap. In this case, the boundary layers on each of the high-lift components may be attached, but the rapid spreading of the viscous wakes will limit the maximum lift that can be achieved [20,21]. An attempt to improve the flow over a high-lift system by addressing one of these limiting factors may improve the performance, but it will still be limited by the other factors. The goal is to identify AFC implementations with meaningful performance improvements by simultaneously addressing all of these effects.

B. Flow Control Layout for Multi-Element Wing Sections

AFC evaluation for practical high-lift systems has been performed for two wing sections. The first is a conventional airfoil that represents a typical transport airplane. It has been derived from the wing of the McDonnell Douglas MD80 airplane with flap deflections corresponding to takeoff and landing. The airfoil has an 11% thickness ratio, and the flap employs moderate Fowler motion. The

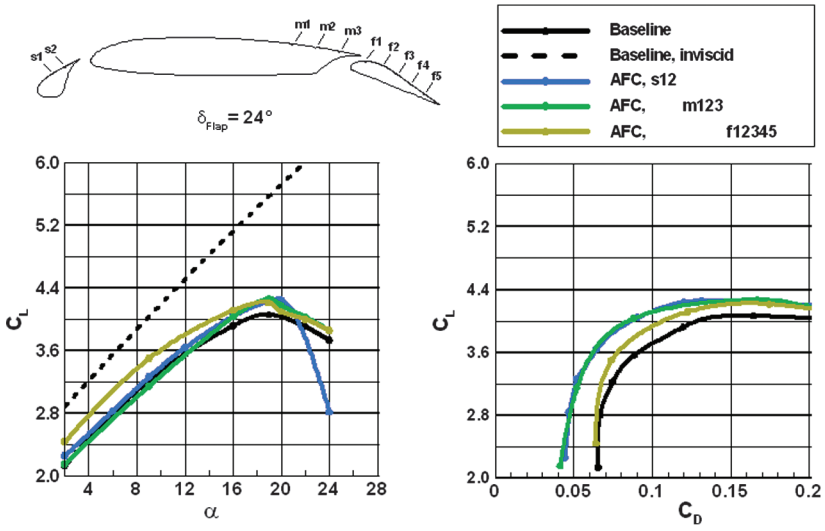

a) Actuation at individual wing components

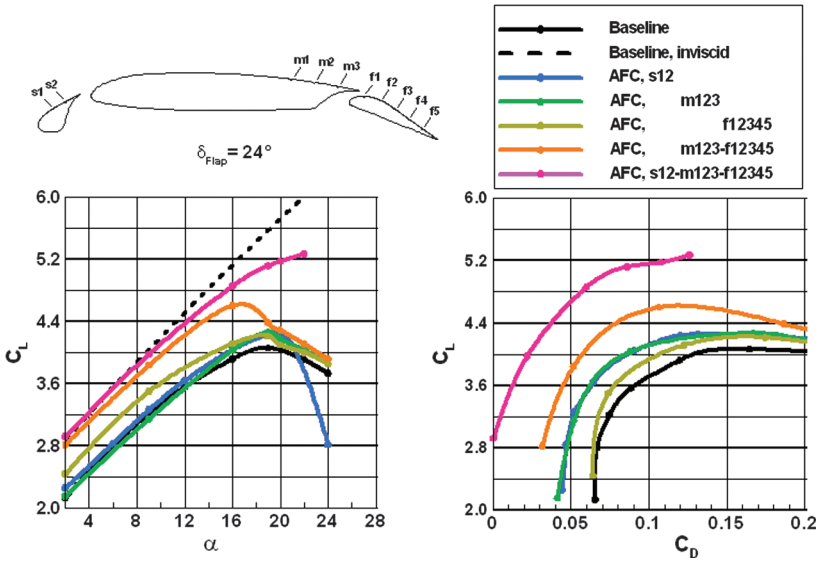

b) Combined actuation

Fig. 5 AFC for the conventional wing section at takeoff flap of 24 deg.

analysis for flap deflections of 13 and 24 deg representing operational takeoff conditions has been performed on a slat/main/flap configuration. For the landing condition, a four-element section has been used with a flap deflection of 40 deg. A vane located between the main element and the flap is used to help maintain attached flow on the flap for this relatively large flap deflection.

The second configuration is an advanced three-element system, which consists of a variable camber Krueger slat and a single 35% chord flap with extensive Fowler motion. This airfoil has been derived from an experimental model that has been thoroughly tested and optimized for very high lift [22]. In the configuration used in this study the original two-element flap system is replaced with a single flap. The supercritical airfoil has a 13% thickness ratio.

The AFC actuation is accomplished with a set of actuators placed on the upper surfaces of the main wing segment and on the movable elements. The port layouts for the two systems are schematically shown in Fig. 1. A set of 10 ports has been used for the conventional section with 2, 3, and 5 ports on the slat, the main, and the flap elements, respectively. This is denoted as a (2, 3, 5) port distribution. The ports are placed in the aft portion of the slat and main elements and five actuators are mounted at equal intervals within the flap. The actuators are positioned such that their respective orifice axes form a 20 deg angle relative to the local upper surface. The advanced high-lift system employs a (2, 5, 5) port configuration. The notation used to describe the multiport AFC pattern identifies the individual wing elements and the respective ports. For example, the system s12–m13–f135 describes an AFC actuation, which employs ports 1 and 2 of the slat, ports 1 and 3 of the main element, and ports 1, 3, and 5 on the flap.

III. Computational Procedure

The numerical tool used for the simulation of high-lift configurations within the context of AFC is a modified version of the OVERFLOW code originally developed by NASA [23]. OVERFLOW is based on the unsteady Reynolds-averaged Navier–Stokes formulation for overset grid systems.

The numerical procedure has been modified by Shmilovich and Yadlin [24] in order to facilitate the analysis and development of a family of flow control techniques. Special modules have been developed for the modeling of time-varying boundary conditions to simulate the flow excitation due to control devices. Jet actuation is described by the mass flow rate, cross-sectional area, and the stagnation pressure and temperature in order to define the velocity at the actuator nozzle. The numerical algorithm uses the characteristics approach for consistent application of the boundary conditions. The

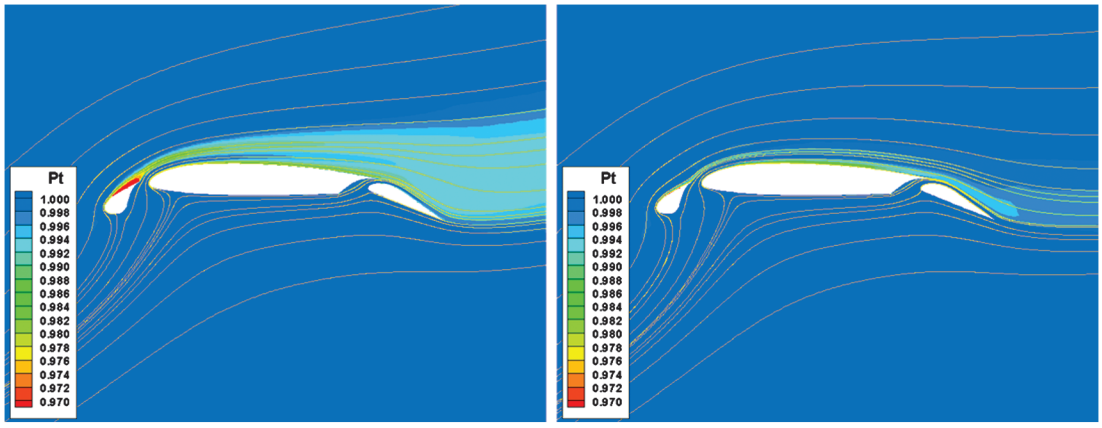

C_L =4.06
Baseline

C_L =5.12
AFC actuation at slat/main/flap (time averaged)

a) Total pressure

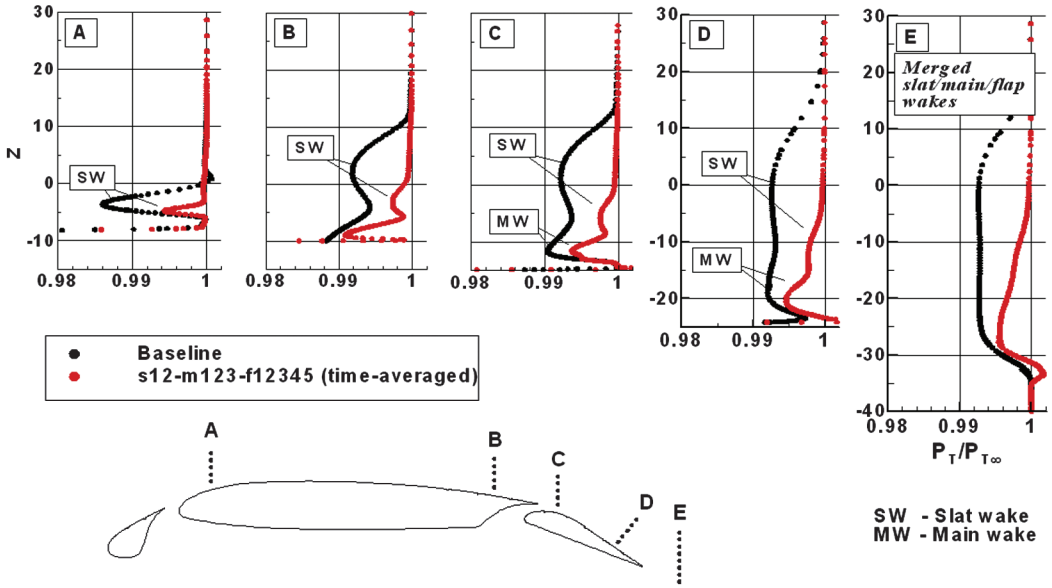

b) Total pressure profiles at select cuts

Fig. 6 Flowfields of the conventional wing section, $\delta_{Flap} = 24$ deg, $\alpha = 19$ deg.

flux vector is aligned with the nozzle axis, and jet pulsation is determined by the forcing frequency.

In this study a second-order upwind differencing scheme and the Spalart–Allmaras turbulence model have been used. The flow control computations use 800 time steps per actuation cycle. The calculation starts with a steady-state solution obtained for the flow in the absence of any actuation. Limit cycle convergence is usually achieved after approximately 45 actuation cycles. At conditions around maximum lift, 70 cycles were required for convergence.

The analysis tool has been validated with experimental data for high-lift configurations with flow control. Lift increments due to AFC obtained at low Reynolds numbers at the Illinois Institute of Technology for a nonslotted flap section [18] are quite well predicted, especially in the linear lift range [24]. Data obtained at the NASA Low Turbulence Pressure Tunnel for a slotted flap configuration with flow control at representative full-scale Reynolds numbers has also been used to validate the computational tool [25]. However, experimental data of AFC for the multi-element wing sections considered in this study is not available. Therefore, validation of the computational tool is only performed for a multi-element airfoil without AFC. The four-element section from which the advanced wing section was derived is used for this purpose. The model was tested in a low-speed wind tunnel with two-dimensional inserts. The lift curves in Fig. 2 show the differences between the experiment and the two-dimensional computed results for a freestream Mach number of 0.1 and chord Reynolds number of 3 million. Good agreement is obtained in the low angle of attack range. However, notable discrepancies exist at high flow incidence. There are several sources of inconsistencies that might explain the discrepancy. With respect to the flow analysis, the computational tool is not accurate at $C_{L\,\max}$ conditions due to shortcomings in turbulence modeling. From the experimental standpoint, because there was no boundary-layer treatment on the inboard surfaces of the inserts, the separation pattern on the airfoil was most likely contaminated by the viscous layers of the inserts. The three-dimensional effects are particularly detrimental for this narrow experimental model with a span-to-chord ratio of 1.125. Another possible inconsistency is transition to turbulent flow. The location of transition from laminar to turbulent flow in the experiment is not known because no tripping of the boundary layers was used. The simulations in Fig. 2, on the other hand, were obtained for fully turbulent flows. However, numerical experiments aimed at obtaining solution sensitivities to transition location indicate that the discrepancies in Fig. 2 can not be attributed to variations in transition location. Moreover, at this particular Reynolds number the occurrence of a laminar separation bubble is not physically

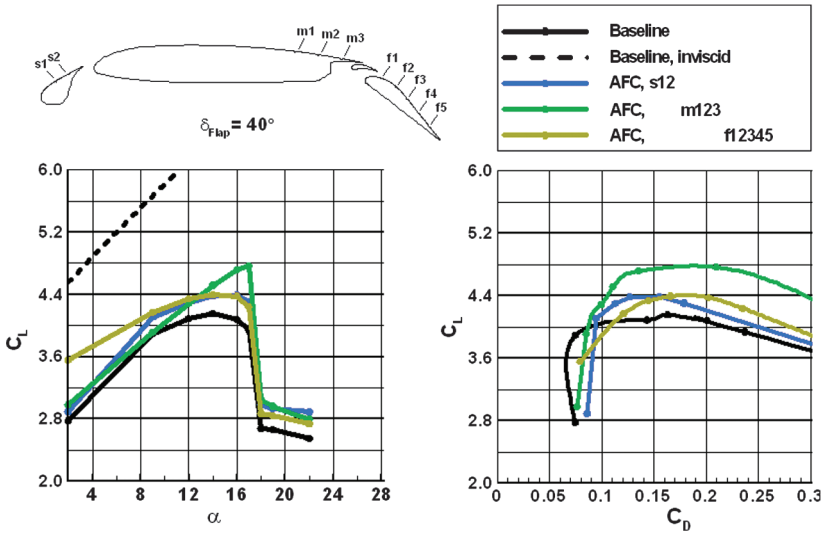

a) Actuation at individual wing components

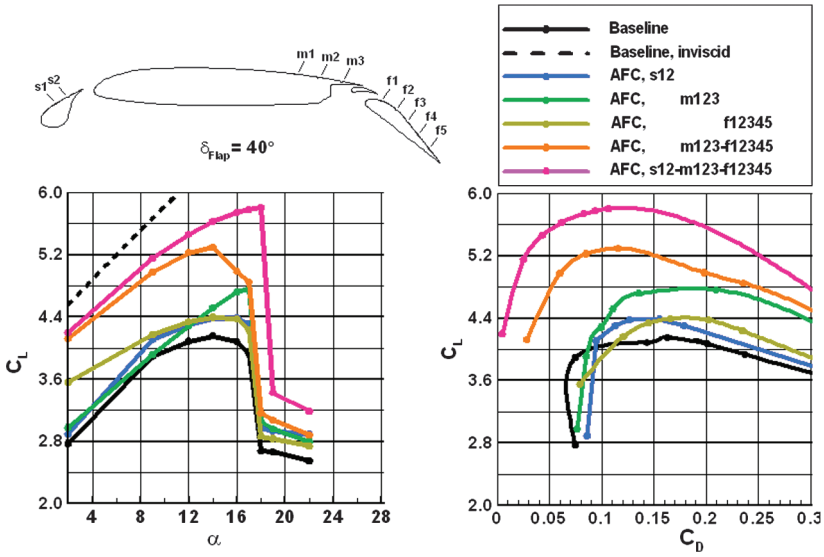

b) Combined actuation

Fig. 7 AFC for the conventional wing section at landing flap of 40 deg.

possible. This is also inferred from examination of the experimental pressure distributions.

Based on the validation against the three sets of experimental data [22,24,25], the computational tool is deemed adequate for the prediction of lift increments due to AFC, and it will be used next for investigating AFC for multi-element wing sections.

IV. Flow Control Analysis

A systematic approach is used to evaluate sets of flow control patterns for two sets of multi-element wing sections at representative takeoff and landing conditions. Control effectiveness and practical implementations of AFC will also be discussed.

A. Conventional Wing Section

Figure 3 shows the computational grid used for the airfoil in the landing configuration. The mesh consists of several overlapping grid systems that conform to the individual elements and the control ports. The actuators are embedded within the respective airfoil elements and are represented by nozzles with constant cross-sectional width of 0.2% airfoil chord.

In these simulations the jets are simulated by prescribing time-varying dynamic and thermodynamic properties of the fluid at the base of the ports. Zero-mass-flow actuation is defined by sinusoidal pulsation of 20 Hz (F^+ of 1.52) with a maximum Mach number of $M_j = 0.242$ for all ports. In all the simulations out-of-phase actuation is applied at adjacent ports. For example, ports f1, f3, and f5 are at 180 deg phase differential to ports f2 and f4.

In analysis and design of AFC for high-lift systems it is instructive to relate to the corresponding inviscid lift [24]. Inviscid lift determines the theoretical upper limit of an airfoil to produce lift in the absence of viscous effects and can be considered as a design objective for an effective AFC implementation. Throughout the following analysis, the inviscid lift is used to gauge the performance of various actuation patterns.

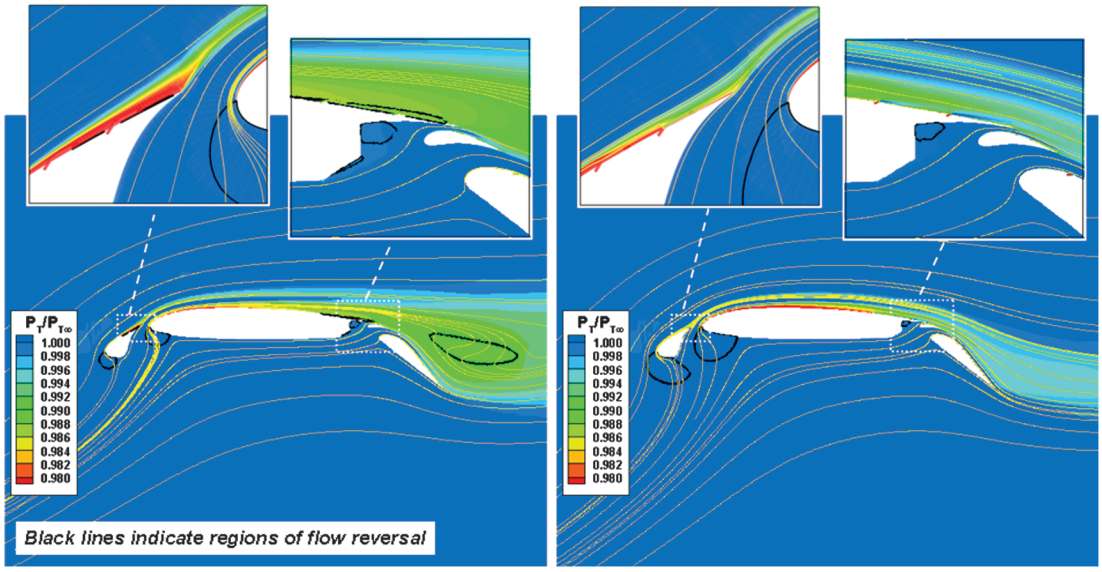

C_L =3.94
Baseline

C_L =5.78
AFC actuation at slat/main/flap (time averaged)

a) Total pressure

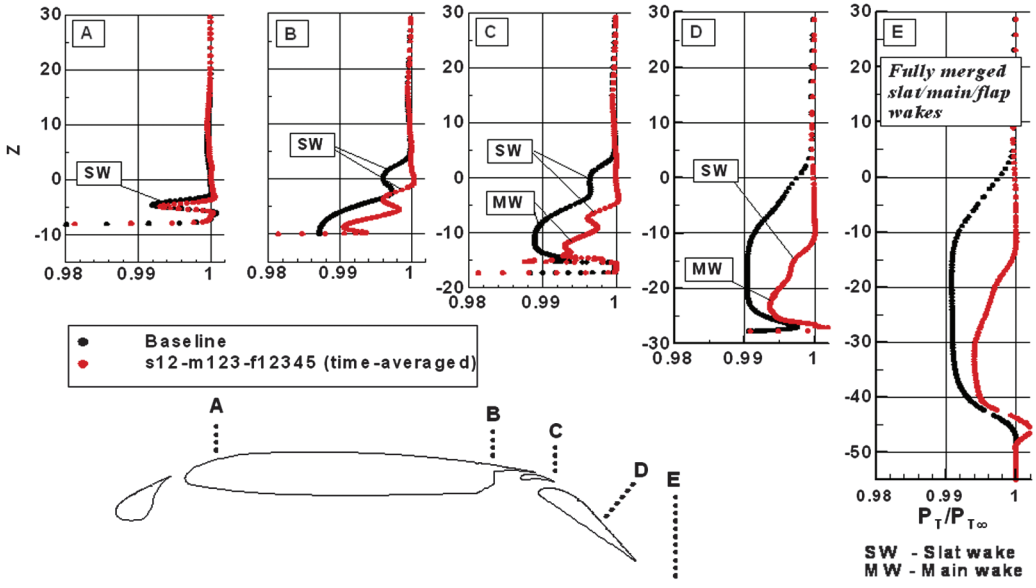

b) Total pressure profiles at select cuts

Fig. 8 Total pressure field for the conventional airfoil, $\delta_{\text{Flap}} = 40$ deg, $\alpha = 17$ deg.

A note on the calculated drag is in order. In the following discussion the forces are based on two-dimensional simulations. Consequently, the induced drag is not accounted for because this component is an artifact of flow past finite wings. Flow control directly impacts the profile drag, but in a general three-dimensional implementation it can also be used to tune the wing span load in order to minimize the induced drag component.

1. *Takeoff Configuration,* $\delta_{\text{Flap}} = 13$ deg

The first set of results is presented for the 13 deg flap deflection, which represents takeoff conditions. The freestream Mach number is 0.1 and the chord Reynolds number is 3 million. For this Mach number the slot momentum coefficient C_μ is 0.015. The calculated forces when AFC is applied separately on the individual elements are shown in Fig. 4a. Of the various flow control modes, the actuation on the main element m123 is notably effective with a $C_{L\,\max} \sim 4.1$ (relative to 3.5 for the baseline). This actuation energizes the nearly separated flow of the main segment and provides added lift. Equally important are favorable effects on the other elements; the extra lift on the main element induces added circulation on the slat and the smaller main wake reduces the displacement effect on the flap. Flap actuation f12345 affects the global circulation resulting in added lift on all elements, but it is less effective than the m123 actuation at higher angles of attack. Finally, slat actuation s12 is essentially ineffectual.

When flow control is applied to both the main and flap elements m123–f12345 the gains are substantial. Figure 4b shows that the lift gain is nearly linear over the range of angles of attack (i.e., the total gain is equivalent to the sum of the individual increments of m123 and f12345). Slat actuation has a profound impact on the stall characteristics when used in conjunction with control on the main and flap elements s12–m123–f12345. The actuation at the slat produces a smaller wake. Consequently, the slat wake traverses the adverse pressure gradient regions of the main and flap without significant degradation in flow quality (i.e., less tendency for off-surface flow reversal). The streamlining effect is significant, resulting in larger turning angle in the aft airfoil portion. The lift is very close to the inviscid level in the linear range. This actuation augments $C_{L\,\max}$ by more than 37%.

It is interesting to note that all AFC patterns that include activation on the main element (m123, m123–f12345, and s12–m123–f12345) are effective. The continual momentum injection supplied by the m123 set energizes the retarded viscous layer in the aft portion of the main element and boosts the load over the entire segment.

2. *Takeoff Configuration,* $\delta_{\text{Flap}} = 24$ deg

The 24 deg flap deflection, which represents an additional takeoff setting, is shown in Fig. 5. According to Fig. 5a, among the AFC applications at the individual elements the flap actuation is the most effective, providing $\Delta CL \sim 0.25$ over the linear range of angles of attack. This implies that the performance of the baseline airfoil is limited by the flap and that the f12345 actuation helps improve the flow in its vicinity. The actuation results in higher circulation on the flap, influencing the global flow and augmenting the circulation on the main segment.

With flap actuation, it is quite likely that the performance-limiting factor shifted elsewhere on the airfoil. To further enhance lift, flow control on the main element is applied in combination with flap actuation (m123–f12345). This mode proves very effective. Contrary to the lower flap deflection, substantial nonlinear lift augmentation is realized as indicated in Fig. 5b. The performance limiting factor of the f12345 case is limited by the flow on the main segment. Thereby, the flow is considerably improved by adding main element actuation. The continual momentum injection supplied by m123 energizes the retarded viscous layer in the aft portion of the main element and boosts the load over the entire segment.

Finally, flow control on the slat is applied in conjunction with main element and flap actuation s12–m123–f12345. This has a profound impact on the stall characteristics with significant increment in $C_{L\,\max}$. The flow control mechanism due to actuation is examined in Fig. 6, which shows the total pressure fields and profiles at select cuts for the baseline and the controlled cases at $\alpha = 19$ deg. At this incidence the baseline flow is on the verge of separation at the trailing edge of the slat and in the aft portion of the main element. The solutions indicate that the actuation at the slat reduces the size of its wake considerably. Consequently, the slat wake traverses the adverse pressure gradient regions of the main and flap without significant degradation in flow quality. This results in lesser tendency for off-surface flow reversal, streamlined flow around the flap, and higher circulation. The streamlining effect is significant, resulting in a larger turning angle in the aft airfoil portion. The total pressure profiles at section E indicate that AFC results in a very narrow wake with a significant reduction in P_T loss, consistent with the drag polars in Fig. 5a (AFC results in approximately 50% reduction in drag).

3. *Landing Configuration,* $\delta_{\text{Flap}} = 40$ deg

Figures 7 and 8 present the results obtained for the landing flap deflection of 40 deg. Here, the AFC application at the main element is notable at high angles of attack, resulting in sizeable improvement in $C_{L\,\max}$. The viscous layer in the baseline case is separated in the trailing-edge region of the main element and off the flap surface (Fig. 8a). In a time-average sense, the momentum engendered by the actuation results in a well behaved boundary layer compared with the baseline flow. The ensuing wake off the main element is narrower and it has smaller velocity deficit. Consequently, the flow is able to better sustain the adverse pressure gradient across the flap and higher flow turning results in added circulation. The addition of actuation at the flap exhibits strong nonlinear effects (m123–f12345). The combined three-element actuation s12–m123–f12345 is very effective over a wider range of flow incidence with notable stall improvement. Full actuation eliminates the off-surface separation

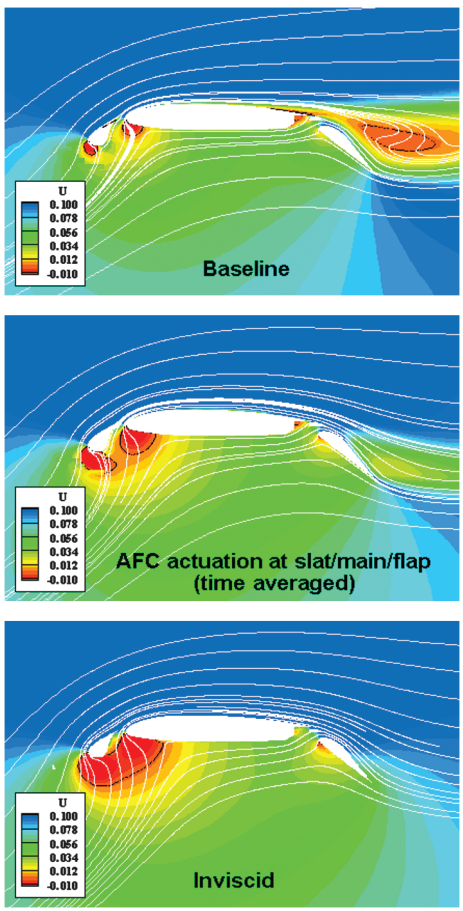

Fig. 9 Resemblance of AFC flow structure to that of an inviscid field (streamlines and contours of streamwise component of velocity, $\delta_{\text{Flap}} = 40$ deg, $\alpha = 17$ deg).

bubble, and it provides streamlined flow even on the highly deflected flap. The stronger circulation is consistent with the high lift level.

The flow structure for the baseline case and the three-element actuation is also described in Fig. 9 at near $C_{L\,\max}$ ($\alpha = 17$ deg). Here the inviscid field is also shown for reference. The time-averaged streamlining effect due to full actuation resembles the inviscid field, consistent with the corresponding lift levels.

4. *Coupled AFC Effects*

The interaction among the individual elements and their wakes is strongly coupled, and it can be favorably affected by combined actuation. Lift augmentation due to AFC can be examined by considering the relative contributions from the actuation at each element. The total lift gain can be expressed in terms of its components

$$\Delta C_{L(S,M,F)} = (C_{L\,\text{AFC–On}} - C_{L\,\text{AFC–Off}}) = \Delta S + \Delta M + \Delta F + \underbrace{\Delta SF + \Delta MF + \Delta SM + \Delta SMF}_{\text{Coupling terms}}$$

where the subscripts S, M, and F denote actuation at the respective elements. Here, for example, ΔS is the lift increment due to AFC at the slat, ΔSF is the lift gain due to the interaction between the slat and flap actuation, and ΔSMF represents the coupled effect resulting from actuation at all elements.

The components of total lift gain for the three flap deflections at select angles of attack are presented in Fig. 10 together with the corresponding lift curves. The lift gains are expressed in terms of increments to inviscid lift limits. The effects of AFC for the 13 deg flap deflection are by and large linear. For example, AFC actuation on the main element does not significantly impact the limiting performance factor on the flap and vice versa. At the low angle of attack some nonlinear offsetting effects exist between slat/main and slat/main/flap actuation modes.

Linear interactions exist even at the larger flap deflections, but the lift gains are largely due to salient features in the predominantly nonlinear flows. For $\delta_{\text{Flap}} = 24$ deg, flap actuation is very effective at low angles of attack, especially when it is used in conjunction with main element actuation (ΔMF). Close to $C_{L\,\max}$, the three-element coupling becomes very important. This implies that there are several performance limiting factors that need to be treated simultaneously in order to realize large benefits.

At $\delta_{\text{Flap}} = 40$ deg the largest lift gains in the linear lift range is obtained from coupled main/flap actuation. At higher incidence the ΔMF coupling contribution diminishes and the actuation at the individual elements becomes important ($\Delta S, \Delta M, \Delta F$), together with the three-element coupling effect (ΔSMF).

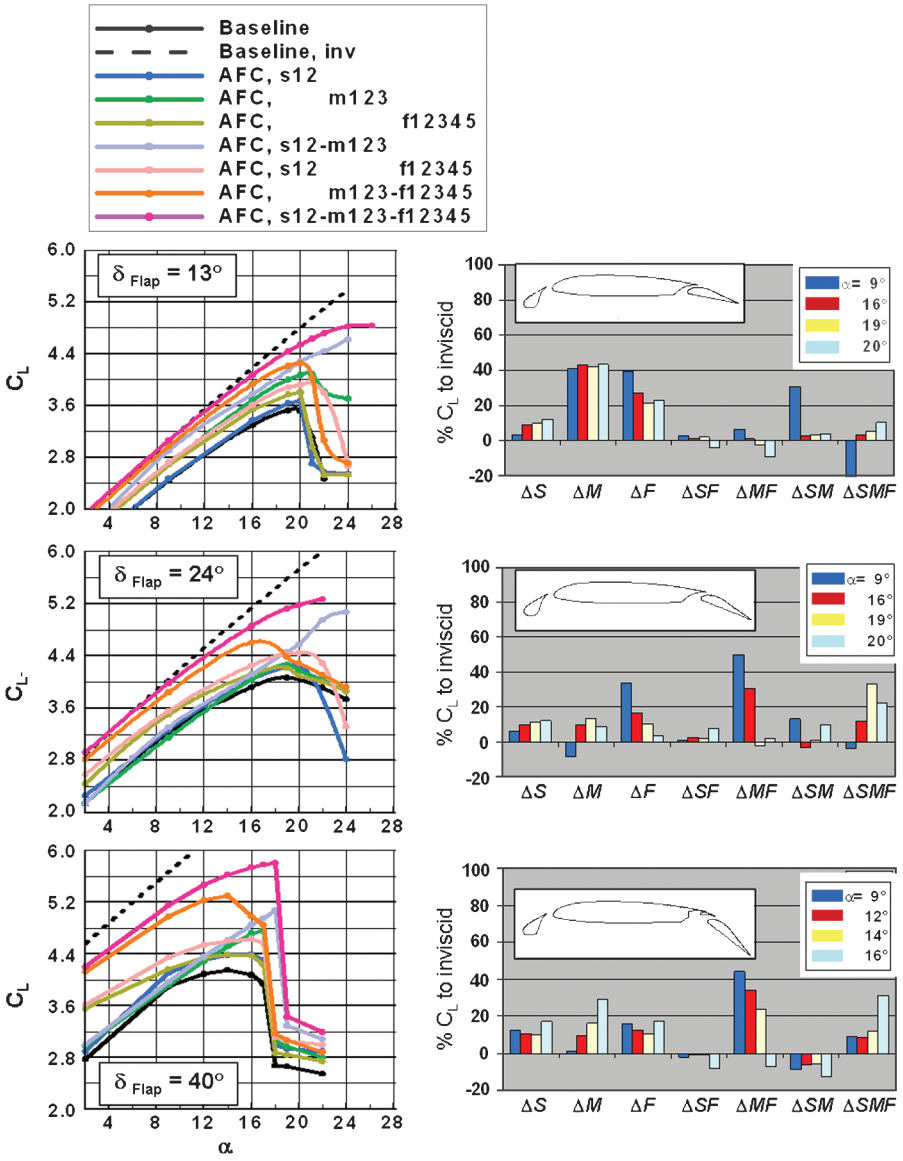

Fig. 10 Contributions to total lift resulting from the interactive flow due to AFC.

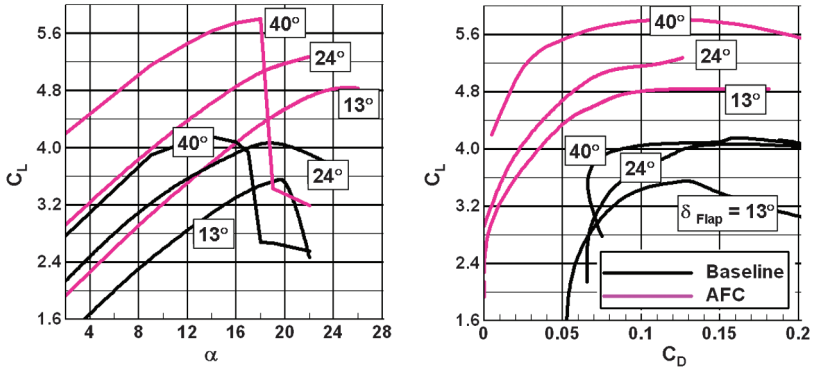

Fig. 11 Relative effects on high-lift performance due to flap deflection and AFC actuation.

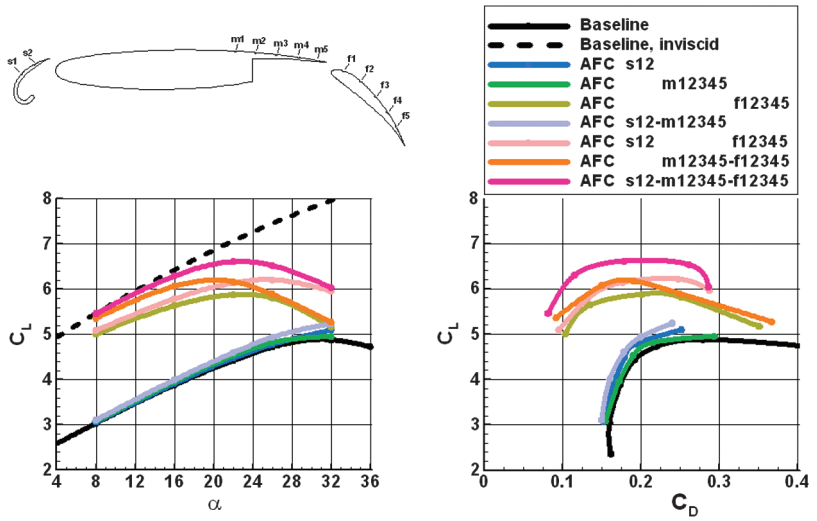

Fig. 12 AFC for the advanced wing section at landing flap of 50 deg.

5. Analogy Between AFC and Flap Deflection

Because the object of both AFC and flap is to boost high-lift performance, it is useful to put their relative merits in perspective. Figure 11 shows that generally in the linear lift range AFC actuation is equivalent to increased flap deflection. Specifically, the actuation for $\delta_{\text{Flap}} = 13$ deg generates lift augmentation similar to that obtained with the 24 deg flap deflection (without flow control). Similarly, AFC for the 24 deg flap configuration produces lift comparable to the level obtained with 40 deg flap deflection. The flow control acts as flaps but with two major advantages: reduced drag and improved stall characteristics.

B. Advanced Wing Section

Figures 12–14 show the aerodynamic parameters for the 50 deg flap deflection and the (2, 5, 5) port configuration. This is representative of landing conditions in which the flow is separated over most of the flap even at low angles of attack. Clearly, the flow at the flap is the main performance-limiting factor. Indeed, the results indicate that out of the actuation at the individual elements, flap actuation is the most effective especially in the linear lift range. The lift can be further boosted by turning on main wing actuation, thus enhancing global circulation and energizing its wake. Adding slat actuation improves the flow at the higher incidence with lift closer to the inviscid levels. The combined actuation results in smooth and attached flow around all elements. The circulation increases on all elements as indicated by the counterclockwise movement of the stagnation points. Relative to the flap contribution to total lift, the coupled actuation effects are more pronounced at high flow incidence. For example, for the uncontrolled case the flap separation is the major performance inhibitor at $\alpha = 26$ deg ($\Delta F \sim 40\%$), but the actuation at the slat boosts performance by producing a wake that favorably interacts with the flow on the flap (note the coupling terms ΔSF and ΔSMF in Fig. 13).

C. Practical AFC Applications

The computations described previously employ sets of actuation ports at individual wing elements in order to identify potential high-lift benefits. For practical implementations, however, it is important to explore ways of minimizing the required input to the flowfield while still achieving large lift increments. This will also have important ramifications to practical integration in terms of weight, compactness, system complexity, structural integrity, power requirement, and maintenance. To demonstrate whether fewer ports can still generate meaningful lift levels, the following actuation patterns have been simulated.

First, the 6-port AFC pattern s12–m23–f45 has been used for the conventional wing section, and the results are shown in Fig. 15. Compared with the full AFC actuation, the 6-port set results in

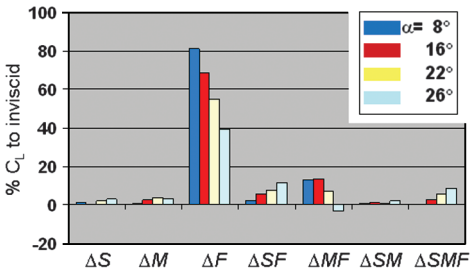

Fig. 13 Contribution to lift from AFC application at individual elements.

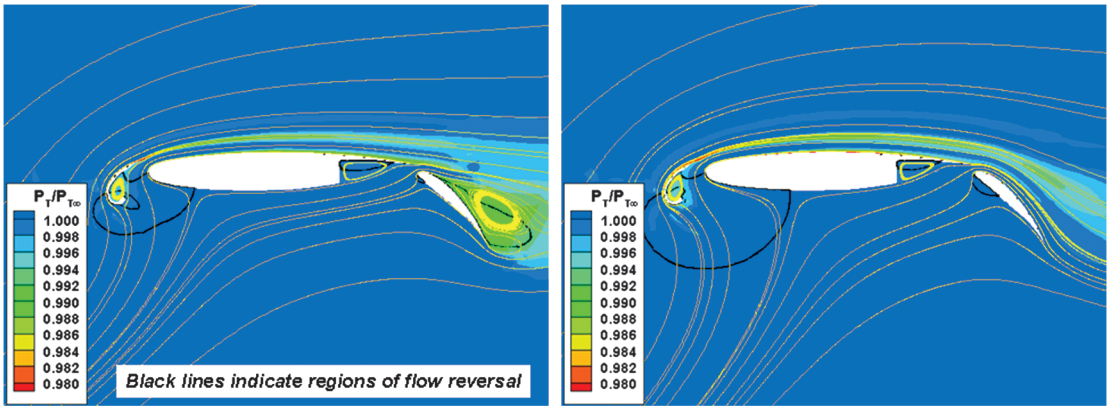

Fig. 14 Total pressure field showing impact of AFC on confluent viscous layers ($\alpha = 22$ deg).

relatively small degradation in lift for all flap deflections, with slightly larger differences for the landing configuration.

A 4-ports set has been investigated for the advanced wing section. The performance is shown in Fig. 16 using the s2–m2–f24 set, which reduces the lift in the linear range to about 70% of the level obtained with the full 12-port actuation, with a commensurate drop in maximum lift.

The purpose of the current study was to provide insight into AFC flow mechanisms and to establish guidelines to port placement at individual wing sections. The goal in the previous exercise in Figs. 15

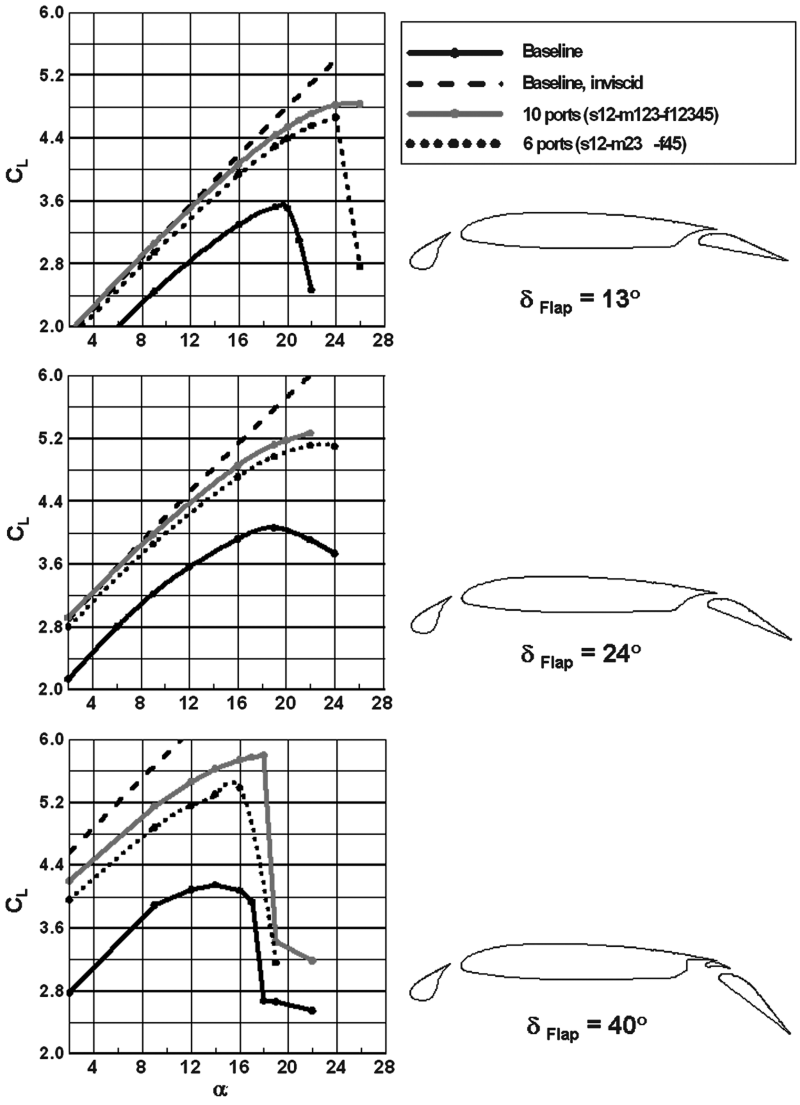

Fig. 15 AFC performance with reduced number of ports (conventional wing section).

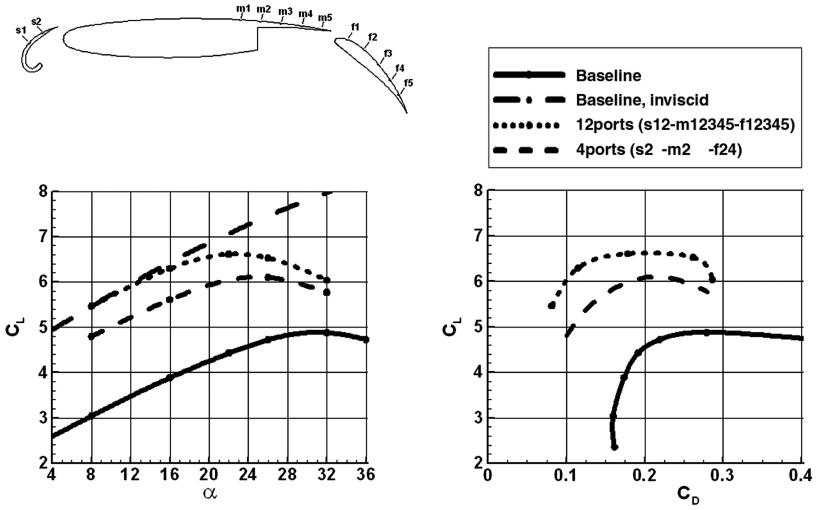

Fig. 16 AFC performance with reduced number of ports (advanced wing section).

and 16 was to demonstrate that it is possible to achieve meaningful lift increments using fewer numbers of ports. It is plausible that smaller inputs to the flowfield could be further achieved by regulating the jet intensity, frequency, and signal phase at individual ports.

V. Conclusions

There are high payoffs for a vehicle that can operate from very short fields, from both economical and operational standpoints. AFC technology has the potential to expand the performance envelope of practical high-lift systems to meet the requirements for takeoff and landing, and it presents a great opportunity for the next generation of airplanes. This study describes a distributed AFC technique for achieving meaningful lift augmentation for multi-element wing sections of realistic transports. Substantial gains in aerodynamic efficiency can be realized by exploiting synergistic effects using actuation at individual wing elements. Depending on the flow conditions, the full benefit of nonlinear augmentation is realized when the actuation is simultaneously applied at select ports. The current study demonstrates that AFC ports can be placed in a way that maximizes their cumulative effectiveness, leading to lift levels approaching the inviscid limit.

References

[1] Washburn, A. E., Gorton, S. A., and Anders, S., "*A Snapshot of Active Flow Control Research at NASA Langley*," AIAA Paper 2002-3155, 2002.

[2] Sellers, W. L., III, Jones, G. S., and Moore, M. D., "Flow Control at NASA Langley in Support of High-Lift Augmentation," AIAA Paper 2002-6006, 2002.

[3] Gorton, S. A., Jenkins, L., and Allan, B., "Active Flow Control on a Boundary-Layer-Ingesting Inlet," AIAA Paper 2004-1203, 2004.

[4] Wygnanski, I., "The Variables Affecting the Control of Separation by Periodic Excitation," AIAA Paper 2004-2505, 2004.

[5] Tilmann, C. P., Kimmel, R. L., Addington, G. A., and Myatt, J. H., "Flow Control Research and Applications at the AFRL's Air Vehicles Directorate," AIAA Paper 2004-2622, 2004.

[6] Anders, S. G., Sellers, W. L., III, and Washburn, A. E., "Active Flow Control Activities at NASA Langley," AIAA Paper 2004-2623, 2004.

[7] Kibens, V., and Bower, W. W., "An Overview of Active Flow Control Applications at the Boeing Company," AIAA Paper 2004-2624, 2004.

[8] Vukasinovic, B., Brzozowski, D., and Glezer, A., "Separation Control over a Surface-Mounted Hemispherical Shell," AIAA Paper 2005-4878, 2005.

[9] Smith, D. R., Amitay, M., Kibens, V., Parekh, D., and Glezer, A., "Modification of Lifting Body Aerodynamics Using Synthetic Jet Actuators," AIAA Paper 1998-0209, 1998.

[10] Chatlynne, E., Rumigny, N., Amitay, M., and Glezer, A., "Virtual Aero-Shaping of a Clark-Y Airfoil Using Synthetic Jet Actuators," AIAA Paper 2001-732, 2001.

[11] Amitay, M., Smith, D. R., Kibens, V., Parekh, D. E., and Glezer, A., "Aerodynamic Flow Control over an Unconventional Airfoil Using Synthetic Jet Actuators," *AIAA Journal*, Vol. 39, No. 3, 2001, pp. 361–370. doi:10.2514/2.1323

[12] Greenblatt, D., and Wygnanski, I., "Effect of Leading-Edge Curvature on Airfoil Separation Control," *Journal of Aircraft*, Vol. 40, No. 3, 2003, pp. 473–481. doi:10.2514/2.3142

[13] Gilarranz, J. L., Traub, L. W., and Rediniotis, O. K., "A New Class of Synthetic Jet Actuators-Part II: Application to Flow Separation Control," *Journal of Fluids Engineering*, Vol. 127, No. 2, March 2005, pp. 377–387. doi:10.1115/1.1882393

[14] Hassan, A., "A Two-Point Active Flow Control Strategy for Improved Airfoil Stall/Post-Stall Aerodynamics," AIAA Paper 2006-0099, 2006.

[15] Spalart, P., Hedges, L., Shur, M., and Travin, A., "Simulation of Active Flow Control on a Stalled Airfoil," *Flow, Turbulence and Combustion*, Vol. 71, Nos. 1–4, 2003, pp. 361–373. doi:10.1023/B:APPL.0000014925.91304.42

[16] Melton, L. P., Yao, C. S., and Seifert, A., "Application of Excitation from Multiple Locations on a Simplified High-Lift System," AIAA Paper 2004-2324, 2004.

[17] Schatz, M., Thiele, F., Petz, R., and Nitsche, W., "Separation Control by Periodic Excitation and its Application to a High Lift Configuration," AIAA Paper 2004-2507, 2004.

[18] Kiedaisch, J., Demanett, B., and Nagib, H., "Active Flow Control Applied to High-Lift Airfoils Utilizing Simple Flaps," AIAA Paper 2006-2856, 2006.

[19] Petz, R., and Nitsche, W., "Active Control of Flow Separation on a Swept Constant Chord Half Model in a High-Lift Configuration," AIAA Paper 2006-3505, 2006.

[20] Smith, A. M. O., "High-Lift Aerodynamics," *Journal of Aircraft*, Vol. 12, No. 6, 1975, pp. 501–530. doi:10.2514/3.59830

[21] Ying, S. X., Spaid, F. W., McGinley, C. B., and Rumsey, C. L., "Investigation of Confluent Boundary Layers in High-Lift Flows," AIAA Paper 1998-2622, 1998.

[22] Strong, J. C., "Operating Report for the Wind Tunnel Test of the Two-Dimensional Supercritical High Lift Development Model LB-437A in the McAir Low Speed Wind Tunnel," McDonnell Douglas Helicopter Systems, Report MDC J6856, St. Louis, MO, 1975.

[23] Buning, P. G., Chiu, I. T., Obayash, S., Rizk, Y. M., and Steger, J. L., "Numerical Simulation of the Integrated Space Shuttle Vehicle in Ascent," AIAA Paper 1988-4359, 1988.

[24] Shmilovich, A., and Yadlin, Y., "Flow Control for the Systematic Buildup of High Lift Systems," *Journal of Aircraft*, Vol. 45, No. 5, 2008, 1680–1688. doi:10.2514/1.35327

[25] Khodadoust, A., and Shmilovich, A., "High Reynolds Numbers Simulations of Distributed Active Flow Control for a High-Lift System," AIAA Paper 2007-4423. 2007.